Spatial extent of an outbreak in animal epidemics

Eric Dumonteil[a], Satya N. Majumdar[b], Alberto Rosso[b,1], and Andrea Zoia[a]

[a]DEN/DM2S/SERMA/LTSD, Commissariat à l'Energie Atomique/Saclay, 91191 Gif-sur-Yvette Cedex, France; and [b]Unité Mixte de Recherche 8626, Centre National de la Recherche Scientifique—Université Paris-Sud, LPTMS, 91405 Orsay Cedex, France

Edited by Susan N. Coppersmith, University of Wisconsin, Madison, WI, and approved January 29, 2013 (received for review July 31, 2012)

Characterizing the spatial extent of epidemics at the outbreak stage is key to controlling the evolution of the disease. At the outbreak, the number of infected individuals is typically small, and therefore, fluctuations around their average are important: then, it is commonly assumed that the susceptible–infected–recovered mechanism can be described by a stochastic birth–death process of Galton–Watson type. The displacements of the infected individuals can be modeled by resorting to Brownian motion, which is applicable when long-range movements and complex network interactions can be safely neglected, like in the case of animal epidemics. In this context, the spatial extent of an epidemic can be assessed by computing the convex hull enclosing the infected individuals at a given time. We derive the exact evolution equations for the mean perimeter and the mean area of the convex hull, and we compare them with Monte Carlo simulations.

branching Brownian motion | extreme value statistics

Models of epidemics traditionally consider three classes of populations—namely, the susceptible (S), the infected (I), and the recovered (R). This framework provides the basis of the so-called SIR model (1, 2), a fully connected mean-field model where the population sizes of the three species evolve with time t by the coupled nonlinear equations: $dS/dt = -\beta IS$, $dI/dt = \beta IS - \gamma I$, and $dR/dt = \gamma I$. Here, γ is the rate at which an infected individual recovers, and β denotes the rate at which it transmits the disease to a susceptible (3–5). In the simplest version of these models, the recovered cannot be infected again. These rate equations conserve the total population size $I(t) + S(t) + R(t) = N$; one assumes that, initially, there is only one infected individual, and the rest of the population is susceptible: $I(0) = 1$, $S(0) = N - 1$, and $R(0) = 0$. Of particular interest is the outbreak stage (i.e., the early times of the epidemic process), when the susceptible population is much larger than the number of infected or recovered. During this regime, for large N, the susceptible population hardly evolves and stays $S(t) \sim N$; therefore, nonlinear effects can be safely neglected, and one can just monitor the evolution of the infected population alone: $dI/dt \sim (\beta N - \gamma)I(t)$. Thus, the ultimate fate of the epidemics depends on the key dimensionless parameter $R_0 = \beta N/\gamma$, which is called the reproduction rate. If $R_0 > 1$, the epidemic explodes and invades a finite fraction of the population; if $R_0 < 1$, the epidemic goes to extinction, and in the critical case $R_0 = 1$ the infected population remains constant (6–8).

This basic deterministic SIR has been generalized to a variety of both deterministic as well as stochastic models, and distinct advantages and shortcomings are discussed at length in refs. 9–11. Generally speaking, stochastic models are more suitable in the presence of a small number of infected individuals, when fluctuations around the average may be relevant (9, 10). During the outbreak of epidemics, the infected population is typically small: in this regime, the evolution can be modeled by resorting to a stochastic birth–death branching process of the Galton–Watson type for the number of infected (9–11), where each infected individual transmits the disease to another individual at rate βN and recovers at rate γ. The epidemic may become endemic for $R_0 > 1$ and becomes extinct for $R_0 < 1$, whereas for $R_0 = 1$ fluctuations are typically long-lived and completely control the time evolution of the infected population (3–5).

How far in space can an epidemic spread? Branching processes alone are not sufficient to describe an outbreak, and spatial effects must necessarily be considered (1, 4, 12–14). Quantifying the geographical spread of an epidemic is closely related to the modeling of the population displacements. Brownian motion is often considered as a paradigm for describing the migration of individuals, despite some well-known shortcomings: for instance, finite speed effects and preferential displacements are neglected. Most importantly, a number of recent studies have clearly shown that individuals geographically far apart can actually be closely related to each other through the so-called small-world connections, such as air traffic, public transportation, and so on; then, the spread of epidemics among humans cannot be realistically modeled without considering these complex networks of interconnections (15–18). Nonetheless, Brownian motion provides a reasonable basis for studying disease propagation in animals and possibly plants (here, pathogen vectors are insects) (5).

Although theoretical models based on branching Brownian motion have provided important insights on how the population size grows and fluctuates with time in a given domain (1, 4, 13, 14), another fundamental question is how the spatial extension of the infected population evolves with time. Assessing the geographical area traveled by a disease is key to the control of epidemics, which is especially true at the outbreak, when confinement and vaccination could be most effective. One major challenge in this very practical field of disease control is how to quantify the area that needs to be quarantined during the outbreak. For animal epidemics, this issue has been investigated experimentally (for instance, in the case of equine influenza) (19). The most popular and widely used method consists of recording the set of positions of infected animals and, at each time instant, constructing a convex hull (i.e., a minimum convex polygon surrounding the positions; a precise definition of the convex hull is given below) (Fig. 1). The convex hull at time t then provides a rough measure of the area over which the infections have spread up to time t. The convex hull method is also used to estimate the home range of animals (i.e., the territory explored by a herd of animals during their daily search for food) (20, 21).

In this paper, we model the outbreak of an epidemic as a Galton–Watson branching process in presence of Brownian spatial diffusion. Despite infection dynamics being relatively simple, the corresponding convex hull is a rather complex function of the trajectories of the infected individuals up to time t, whose statistical properties seem to be a formidable problem. Our main goal is to characterize the time evolution of the convex hull associated with this process, particularly its mean perimeter and area.

The rest of the paper is organized as follows. We first describe precisely the model and summarize our main results. Then, we provide a derivation of our analytical findings supported by extensive numerical simulations. We conclude with perspectives and discussions. Some details of the computations are relegated to *SI Text*.

Author contributions: E.D., S.N.M., A.R., and A.Z. performed research and wrote the paper.

The authors declare no conflict of interest.

This article is a PNAS Direct Submission.

[1]To whom correspondence should be addressed. E-mail: alberto.rosso@u-psud.fr.

This article contains supporting information online at www.pnas.org/lookup/suppl/doi:10.1073/pnas.1213237110/-/DCSupplemental.

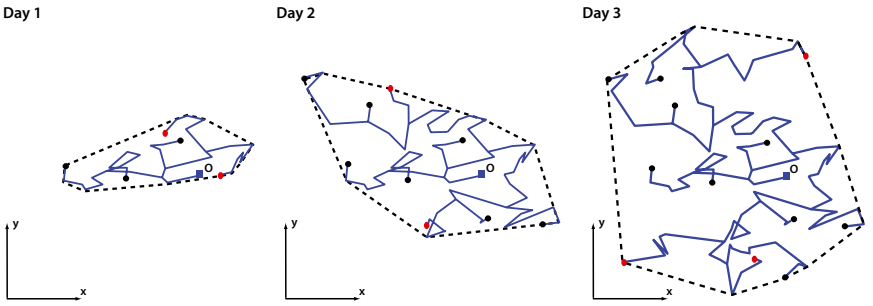

Fig. 1. The snapshots of the trajectories of an assembly of infected individuals at the epidemics outbreak at three different times (schematic) starting from a single infected at the origin O at time $t = 0$. Individuals that are still infected at a given time t are displayed as red dots, whereas individuals already recovered are shown as black dots. The convex hull enclosing the trajectories (shown as a dashed line) is a measure of the geographical area covered by the spreading epidemic. As the epidemic grows in space, the associated convex hull also grows in time.

Model and Main Results

Consider a population of N individuals uniformly distributed in a 2D plane, with a single infected at the origin at the initial time. At the outbreak, it is sufficient to keep track of the positions of the infected, which will be marked as particles. The dynamics of the infected individuals are governed by the following stochastic rules. In a small time interval dt, each infected alternatively has three actions.

i) The infected individual recovers with probability γdt. This event corresponds to the death of a particle with rate γ.

ii) The infected individual infects, by local contact, a new susceptible individual from the background with probability bdt. This event corresponds to the birth of a new particle that can subsequently diffuse. The originally infected particle still remains infected, which means that the trajectory of the originally infected particle branches into two new trajectories. The rate b replaces the rate βN in the SIR or the Galton–Watson process mentioned before.

iii) The infected individual diffuses with diffusion constant D with probability $1 - (\gamma + b)dt$. The coordinates $\{x(t), y(t)\}$ of the particle get updated to the new values $\{x(t) + \eta_x(t)dt, y(t) + \eta_y(t)dt\}$, where $\eta_x(t)$ and $\eta_y(t)$ are independent Gaussian white noises with zero mean and correlators $\langle \eta_x(t)\eta_x(t')\rangle = 2D\delta(t - t')$, $\langle \eta_y(t)\eta_y(t')\rangle = 2D\delta(t - t')$, and $\langle \eta_x(t)\eta_y(t')\rangle = 0$.

The only dimensionless parameter in the model is the ratio $R_0 = b/\gamma$ (i.e., the basic reproduction number).

Consider now a particular history of the assembly of the trajectories of all of the infected individuals up to time t, starting from a single infected initially at the origin (Fig. 1). For every realization of the process, we construct the associated convex hull C. To visualize the convex hull, imagine stretching a rubber band so that it includes all of the points of the set at time t inside it and then releasing the rubber band. It shrinks and finally gets stuck when it touches some points of the set; therefore, it cannot shrink any more. This final shape is precisely the convex hull associated with this set.

In this paper, we show that the mean perimeter $\langle L(t)\rangle$ and the mean area $\langle A(t)\rangle$ of the convex hull are ruled by two coupled nonlinear partial differential equations that can be solved numerically for all t (Fig. 2). The asymptotic behavior for large t can be determined analytically for the critical ($R_0 = 1$), subcritical ($R_0 < 1$), and supercritical ($R_0 > 1$) regimes. In particular, in the critical regime, the mean perimeter saturates to a finite value as $t \to \infty$, whereas the mean area diverges logarithmically for large t:

$$\langle L(t \to \infty)\rangle = 2\pi\sqrt{\frac{6D}{\gamma}} + \mathcal{O}\left(t^{-1/2}\right) \qquad [1]$$

and

$$\langle A(t \to \infty)\rangle = \frac{24\pi D}{5\gamma}\ln t + \mathcal{O}(1). \qquad [2]$$

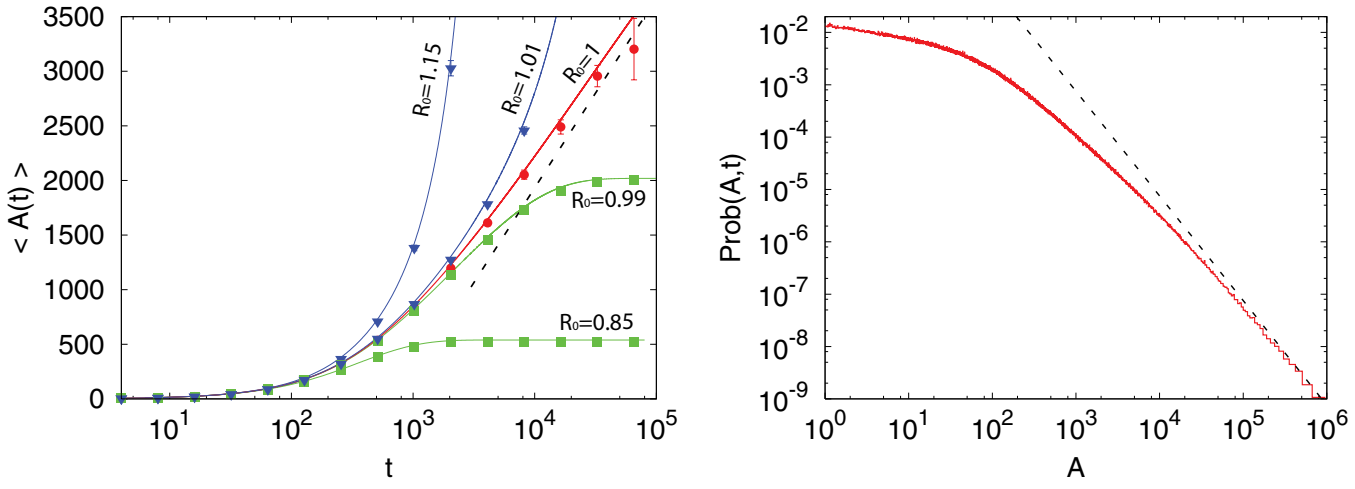

Fig. 2. (*Left*) The average area $\langle A(t)\rangle$ of the convex hull as a function of the observation time. For the parameter values, we have chosen $D = 1/2$ and $b = R_0\gamma = 0.01$. We considered five different values of R_0. We have obtained these results by two different methods. (*i*) One method is by the numerical integration of Eqs. **9** and **14** and using Eq. **15**. These results are displayed as solid lines. (*ii*) The other method is by Monte Carlo simulations of the 2D branching Brownian motion with death with the same parameters averaged over 10^5 samples. Monte Carlo simulations are displayed as symbols. The dashed lines represent the asymptotic limits as given in Eq. **2** for the critical case $R_0 = 1$. Additional details of the numerical simulations are provided in *SI Text*. (*Right*) Distribution of the area of the convex hull for the critical case $R_0 = 1$, with $\gamma = 0.01$ and $D = 1/2$, as obtained by Monte Carlo simulations with 2×10^6 realizations. The dashed line corresponds to the power-law $(24\pi D/5\gamma)A^{-2}$ as predicted by expression **20**.

This prediction seems rather paradoxical at a first glance. How can the perimeter of a polygon be finite while its area is divergent? The resolution to this paradox owes its origin precisely to statistical fluctuations. The results in Eqs. **1** and **2** are true only on average. Of course, for each sample, the convex hull has a finite perimeter and a finite area. However, as we later show, the probability distributions of these random variables have power-law tails at long time limits. For instance, although $\mathrm{Prob}(L, t\to\infty)\sim L^{-3}$ for large L (thus leading to a finite first moment), the area distribution behaves as $\mathrm{Prob}(A, t\to\infty)\sim A^{-2}$ for large A. Hence, the mean area is divergent as $t\to\infty$ (Fig. 2).

When $R_0\neq 1$, the evolution of the epidemic is controlled by a characteristic time t^*, which scales like $t^*\sim |R_0-1|^{-1}$. For times $t<t^*$ the epidemic behaves as in the critical regime. In the subcritical regime, for $t>t^*$, the quantities $\langle L(t)\rangle$ and $\langle A(t)\rangle$ rapidly saturate, and the epidemic goes eventually to extinction. In contrast, in the supercritical regime (which is the most relevant for virulent epidemics that spread fast), a new time-dependent behavior emerges when $t>t^*$, because there exists a finite probability (namely $1-1/R_0$) that the epidemic never goes to extinction (Fig. 3). More precisely, we later show that

$$\left\langle L\left(t\gg t^*\right)\right\rangle = 4\pi\left(1-\frac{1}{R_0}\right)\sqrt{D\gamma(R_0-1)}\,t \qquad [3]$$

and

$$\left\langle A\left(t\gg t^*\right)\right\rangle = 4\pi\left(1-\frac{1}{R_0}\right)D\gamma\,(R_0-1)t^2. \qquad [4]$$

The ballistic growth of the convex hull stems from an underlying traveling front solution of the nonlinear equation governing the convex hull behavior. Indeed, the prefactor of the perimeter growth is proportional to the front velocity $v^*=2\sqrt{D\gamma(R_0-1)}$. As time increases, the susceptible population decreases because of the growth of the infected individuals: this depletion effect leads to a breakdown of the outbreak regime and a slowing down of the epidemic propagation.

Statistics of the Convex Hull

Characterizing the fluctuating geometry of C is a formidable task even in absence of branching ($b=0$) and death ($\gamma=0$), i.e., purely for diffusion process in 2Ds. Major recent breakthroughs have, nonetheless, been obtained for diffusion processes (22, 23) by a clever adaptation of the Cauchy integral geometric formulae (24, 25) for the perimeter and area of any closed convex curve in 2Ds. In fact, the problem of computing the mean perimeter and area of the convex hull of any generic 2D stochastic process can be mapped, using Cauchy formulae, to the problem of computing the moments of the maximum and the time at which the maximum occurs for the associated 1D component stochastic process (22, 23). This technique was used for computing the mean perimeter and area of the convex hull of a 2D regular Brownian motion (22, 23) and a 2D random acceleration process (26).

Our main idea here is to extend this method to compute the convex hull statistics for the 2D branching Brownian motion. Using this general mapping and isotropy in space (*SI Text*), the average perimeter and area of the convex hull are given by

$$\langle L(t)\rangle = 2\pi\langle x_m(t)\rangle \qquad [5]$$

and

$$\langle A(t)\rangle = \pi\left[\left\langle x_m^2(t)\right\rangle - \left\langle y^2(t_m)\right\rangle\right], \qquad [6]$$

where x_m is the maximum displacement of our 2D stochastic process in the x direction up to time t, t_m is the time at which the maximum displacement along x direction occurs, and $y(t_m)$ is the ordinate of the process at t_m (i.e., when the displacement along the x direction is maximal). A schematic representation is provided in Fig. 4, where the global maximum x_m is achieved by one single infected individual, whose path is marked in red. A crucial observation is that the y component of the trajectory connecting O to this red path is a regular 1D Brownian motion. Hence, given t_m and t, clearly $\langle y^2(t_m)\rangle = 2D\langle t_m\rangle$. Therefore,

$$\langle A(t)\rangle = \pi\left[\left\langle x_m^2(t)\right\rangle - 2D\langle t_m(t)\rangle\right]. \qquad [7]$$

Eqs. **5** and **7** thus show that the mean perimeter and area of the epidemics outbreak are related to the extreme statistics of a 1D branching Brownian motion with death. Indeed, if we can compute the joint distribution $P_t(x_m, t_m)$, we can, in turn, compute the three moments $\langle x_m\rangle$, $\langle x_m^2\rangle$, and $\langle t_m\rangle$ that are needed in Eqs. **5** and **7**. We show below that this calculation can be performed exactly.

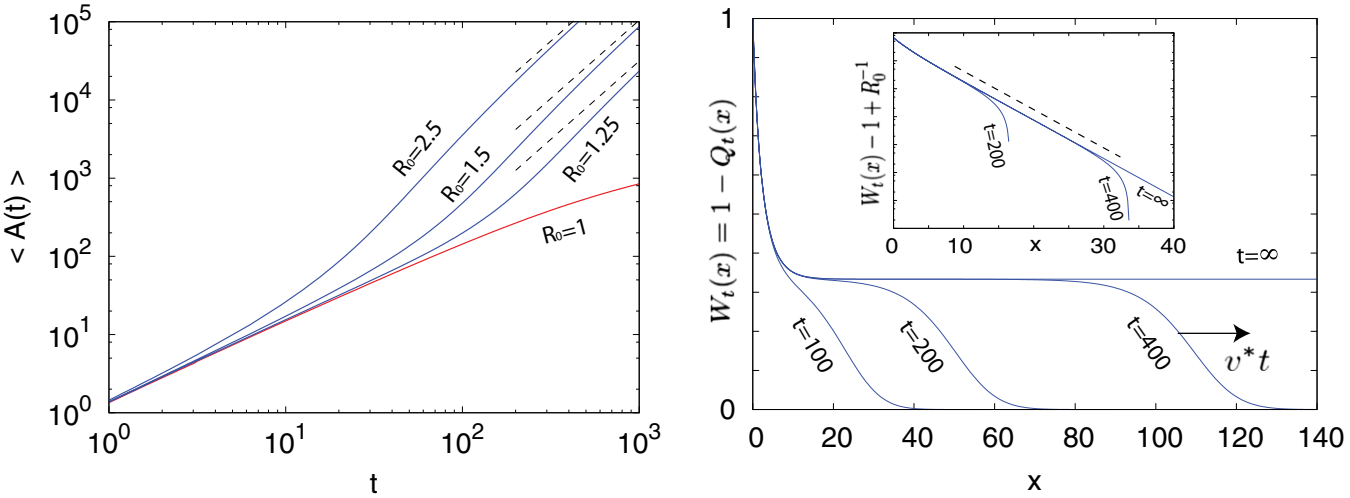

Fig. 3. (*Left*) The time behavior of the average area in the supercritical regime for different values of $R_0>1$. Dashed lines represent the asymptotic scaling as in Eq. **4**. The red curve corresponds to the critical regime. (*Right*) The behavior of $W_t(x)=1-Q_t(x)$ for $R_0=1.5$ at different times as in Eq. **21**. When $t\to\infty$, $W_t(x)\to 1-R_0^{-1}$, and for large but finite times, the traveling front behavior is clearly visible. *Inset* displays the exponential convergence of $W_t(x)$ to the asymptotic limit. The dashed line represents $\xi=\sqrt{D/\gamma(R_0-1)}$.

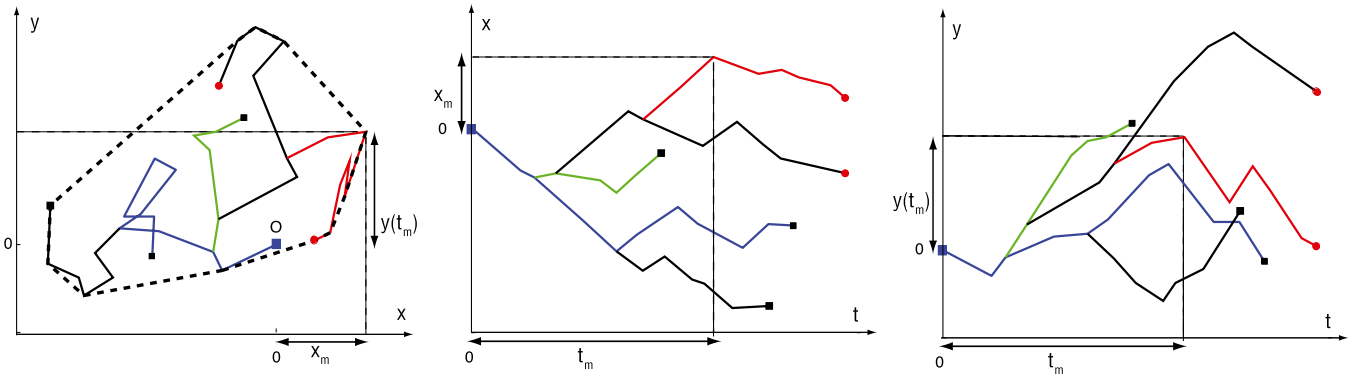

Fig. 4. (*Left*) A branching random walk composed of five individuals. At time $t = 0$, a single infected individual is at the origin O and starts diffusing (blue line). At later times, this individual branches and gives rise to other infected individuals. Among these individuals, the red path reaches the maximum x_m along the x component up to the final time t. infected individuals at a given time t are displayed as red dots, whereas recovered individuals are displayed as black dots. (*Center*) The displacement along the x direction as a function of time. The red path reaches the global maximum x_m at time t_m. (*Right*) The displacement along the y direction as a function of time. When the red path reaches the global maximum x_m at time t_m, its y coordinate attains the value $y(t_m)$. A crucial observation is that the y component of the trajectory connecting O to the red path is a regular Brownian motion. This observation does not apply to the x component, which is constrained to reach the global maximum of the branching process.

Convex Hull Perimeter and Maximum x_m. For the average perimeter, we just need the first moment $\langle x_m(t)\rangle = \int_0^\infty x_m q_t(x_m) dx_m$, where $q_t(x_m)$ denotes the probability density of the maximum of the 1D component process. It is convenient to consider the cumulative distribution $Q_t(x_m)$ (i.e., the probability that the maximum x displacement stays below a given value x_m up to time t). Then, $q_t(x_m) = dQ_t(x_m)/dx_m$, and $\langle x_m(t)\rangle = \int_0^\infty [1 - Q_t(x_m)] dx_m$. Because the process starts at the origin, its maximum x displacement, for any time t, is necessarily nonnegative (i.e., $x_m \geq 0$). We next write down a backward Fokker–Planck equation describing the evolution of $Q_t(x_m)$ by considering the three mutually exclusive stochastic moves in a small time interval dt: starting at the origin at $t = 0$, the walker during the subsequent interval $[0, dt]$ dies with probability γdt, infects another individual (i.e., branches) with probability $bdt = R_0 \gamma dt$, or diffuses by a random displacement $\Delta x = \eta_x(0) dt$ with probability $1 - \gamma(1 + R_0)dt$. In the last case, its new starting position is Δx for the subsequent evolution. Hence, for all $x_m \geq 0$, one can write

$$Q_{t+dt}(x_m) = \gamma dt + R_0 \gamma dt Q_t^2(x_m) + [1 - \gamma(R_0 + 1)] dt \langle Q_t(x_m - \Delta x)\rangle , \quad [8]$$

where the expectation $\langle\rangle$ is taken with respect to the random displacements Δx. The first term means that if the process dies right at the start, its maximum up to t is clearly zero and hence, necessarily less than x_m. The second term denotes the fact that, in case of branching, the maximum of each branch stays below x_m: because the branches are independent, one gets a square. The third term corresponds to diffusion. By using $\langle \Delta x\rangle = 0$ and $\langle \Delta x^2\rangle = 2Ddt$ and expanding Eq. **8** to the first order in dt and second order in Δx, we obtain

$$\frac{\partial}{\partial t} Q = D \frac{\partial^2}{\partial x_m^2} Q - \gamma(R_0 + 1) Q + \gamma R_0 Q^2 + \gamma \quad [9]$$

for $x_m \geq 0$, satisfying the boundary conditions $Q_t(0) = 0$ and $Q_t(\infty) = 1$ and the initial condition $Q_0(x_m) = \Theta(x_m)$, where Θ is the Heaviside step function. Hence, from Eq. **5**,

$$\langle L(t)\rangle = 2\pi \int_0^\infty [1 - Q_t(x_m)] dx_m . \quad [10]$$

Eq. **9** can be solved numerically for all t and all R_0 values, which allows for subsequent computation of $\langle L(t)\rangle$ in Eq. **10** (details are provided in *SI Text* and Figs. S1, S2, and S3).

Convex Hull Area. To compute the average area in Eq. **7**, we need to evaluate $\langle x_m^2(t)\rangle$ as well as $\langle t_m\rangle$. After the cumulative distribution $Q_t(x_m)$ is known, the second moment $\langle x_m^2(t)\rangle$ can be directly computed by integration, namely $\langle x_m^2(t)\rangle = \int_0^\infty dx_m 2x_m(1 - Q_t(x_m))$. To determine $\langle t_m\rangle$, we need to also compute the probability density $p_t(t_m)$ of the random variable t_m. Unfortunately, writing down a closed equation for $p_t(t_m)$ is hardly feasible. Instead, we first define $P_t(x_m, t_m)$ as the joint probability density that the maximum of the x component achieves the value x_m at time t_m, when the full process is observed up to time t. Then, we derive a backward evolution equation for $P_t(x_m, t_m)$ and integrate out x_m to derive the marginal density $p_t(t_m) = \int_0^\infty P_t(x_m, t_m) dx_m$. Following the same arguments as for $Q_t(x_m)$ yields a backward equation for $P_t(x_m, t_m)$,

$$\begin{aligned} P_{t+dt}(x_m, t_m) = {} & [1 - \gamma(R_0 + 1)dt] \langle P_t(x_m - \Delta x, t_m - dt)\rangle \\ & + 2\gamma R_0 dt Q_t(x_m) P_t(x_m, t_m - dt) \end{aligned} . \quad [11]$$

The first term at the right-hand side represents the contribution from diffusion. The second term represents the contribution from branching: we require that one of them attains the maximum x_m at the time $t_m - dt$, whereas the other stays below x_m [$Q_t(x_m)$ being the probability that this condition is satisfied]. The factor 2 comes from the interchangeability of the particles. Developing Eq. **11** to leading order gives

$$\left[\frac{\partial}{\partial t} + \frac{\partial}{\partial t_m}\right] P_t = \left[D \frac{\partial^2}{\partial x_m^2} - \gamma(R_0 + 1) + 2\gamma R_0 Q_t\right] P_t . \quad [12]$$

This equation describes the time evolution of $P_t(x_m, t_m)$ in the region $x_m \geq 0$ and $0 \leq t_m \leq t$. It starts from the initial condition $P_0(x_m, t_m) = \delta(x_m)\delta(t_m)$ (because the process begins with a single infected with x component located at $x = 0$, it implies that, at $t = 0$, the maximum $x_m = 0$ and also $t_m = 0$). For any $t > 0$ and $x_m > 0$, we have the condition $P_t(x_m, 0) = 0$. We need to also specify the boundary conditions at $x_m = 0$ and $x_m \to \infty$, which read (*i*) $P_t(\infty, t_m) = 0$ (because for finite t, the maximum is necessarily finite) and (*ii*) $P_t(0, t_m) = \delta(t_m)\, q_t(x_m)|_{x_m = 0}$. The latter condition comes from the fact that, if $x_m = 0$, the x component of the entire process, starting at 0 initially, stays below zero in the time interval $[0, t]$, which happens with probability $q_t(x_m)|_{x_m = 0}$: consequently, t_m must necessarily be zero. Furthermore, by integrating $P_t(x_m, t_m)$ with respect to t_m, we recover the marginal density $q_t(x_m)$.

The numerical integration of the full Eq. **12** would be rather cumbersome. Fortunately, we do not need this calculation. Because we are only interested in $\langle t_m \rangle$, it is convenient to introduce

$$T_t(x_m) = \int_0^t t_m P_t(x_m, t_m) dt_m, \qquad [13]$$

from which the average follows as $\langle t_m \rangle = \int dx_m T_t(x_m)$. Multiplying Eq. **12** by t_m and integrating by parts, we get

$$\frac{\partial}{\partial t} T_t - q_t(x_m) = \left[D \frac{\partial^2}{\partial x_m^2} + 2\gamma R_0 Q_t - \gamma(R_0 + 1) \right] T_t \qquad [14]$$

with the initial condition $T_0(x_m) = 0$ and the boundary conditions $T_t(0) = 0$ and $T_t(\infty) = 0$. Eq. **14** can be integrated numerically together with Eq. **9** (details are provided in *SI Text*), and the behavior of

$$\langle A(t) \rangle = \pi \int_0^\infty dx_m [2x_m(1 - Q_t(x_m)) - T_t(x_m)] \qquad [15]$$

as a function of time is illustrated in Fig. 2.

Critical Regime. We now focus on the critical regime $R_0 = 1$. We begin with the average perimeter: for $R_0 = 1$, Eq. **9** admits a stationary solution as $t \to \infty$, which can be obtained by setting $\partial Q/\partial t = 0$ and solving the resulting differential equation. In fact, this stationary solution was already known in the context of the genetic propagation of a mutant allele (27). Taking the derivative of this solution with respect to x_m, we get the stationary probability density of the maximum x_m:

$$q_\infty(x_m) = \partial_{x_m} Q_\infty(x_m) = \frac{2\sqrt{\frac{\gamma}{6D}}}{\left(1 + \sqrt{\frac{\gamma}{6D}} x_m\right)^3}. \qquad [16]$$

The average is $\langle x_m \rangle = \int_0^\infty x_m q_\infty(x_m) dx_m = \sqrt{6D/\gamma}$, which yields Eq. **1** for the average perimeter of the convex hull at late times.

To compute the average area in Eq. **7**, we need to also evaluate the second moment $\langle x_m^2(t) \rangle$, which diverges as $t \to \infty$ because of the power-law tail of the stationary probability density $q_\infty(x_m) \propto x_m^{-3}$ for large x_m. Hence, we need to consider large but finite t. In this case, the time-dependent probability density $q_t(x_m)$ displays a scaling form, which can be conveniently written as

$$q_t(x_m) \simeq q_\infty(x_m) f\left(\frac{x_m}{\sqrt{Dt}}\right), \qquad [17]$$

where $f(z)$ is a rapidly decaying function with $f(z \ll 1) \simeq 1$ and $f(z \gg 1) \simeq 0$. Using the scaling form of expression **17** and Eq. **9**, one can derive a differential equation for $f(z)$. However, it turns out that we do not really need the solution of $f(z)$.

From expression **17**, we see that the asymptotic power-law decay of $q_t(x_m)$ for large x_m has a cutoff around $x_m^* \sim \sqrt{Dt}$ and that $f(z)$ is the cutoff function. The second moment at finite but large times t is given by $\langle x_m^2(t) \rangle = \int_0^\infty x_m^2 \, q_t(x_m) dx_m$. Substituting the scaling form and cutting off the integral over x_m at $x_m^* = c\sqrt{t}$ [where the constant c depends on the precise form of $f(z)$], we get to leading order for large t:

$$\langle x_m^2(t) \rangle \simeq \int_0^{x_m^*} x_m^2 q_\infty(x_m) dx_m \simeq \frac{6D}{\gamma} \ln t. \qquad [18]$$

Thus, interestingly, the leading order result is universal [i.e., independent of the details of the cutoff function $f(z)$; the c dependence is only in the subleading term]. To complete the characterization of $\langle A(t) \rangle$ in Eq. **7**, we still need to determine $\langle t_m \rangle$: in *SI Text*, we explicitly determine the stationary solution $P_\infty(x_m, t_m)$ for $R_0 = 1$. By following the same arguments as for $\langle x_m^2(t) \rangle$, we show that

$$\langle t_m \rangle \simeq \frac{3}{5\gamma} \ln t \qquad [19]$$

for large t, which leads again to a logarithmic divergence in time. Finally, substituting expressions **18** and **19** in Eq. **7** gives the result announced in Eq. **2**.

A deeper understanding of the statistical properties of the process would demand knowing the full distribution $\mathrm{Prob}(L, t)$ and $\mathrm{Prob}(A, t)$ of the perimeter and area. These quantities seem rather hard to compute, but one can obtain the asymptotic tails of the distributions by resorting to scaling arguments. Following the lines of the Cauchy formula (*SI Text*), it is reasonable to assume that, for each sample, the perimeter scales as $L(t) \sim x_m(t)$. We have seen that the distribution of $x_m(t)$ has a power-law tail for large t: $q_\infty(x_m) \sim x_m^{-3}$ for large x_m. Then, assuming the scaling $L(t) \sim x_m(t)$ and using $\mathrm{Prob}(L, t \to \infty) dL \sim q_\infty(x_m) dx_m$, it follows that, at late times, the perimeter distribution also has a power-law tail: $\mathrm{Prob}(L, t \to \infty) \sim L^{-3}$ for large L. Similarly, using the Cauchy formula for the area, we can reasonably assume that, for each sample, $A(t) \sim x_m^2(t)$ in the scaling regime. Once again, using $\mathrm{Prob}(A, t \to \infty) dA = q_\infty(x_m) dx_m$, we find that the area distribution also converges, for large t, to a stationary distribution with a power-law tail: $\mathrm{Prob}(A, t \to \infty) \sim A^{-2}$ for large A. Moreover, the logarithmic divergence of the mean area calls for a precise ansatz on the tail of the area distribution, namely

$$\mathrm{Prob}(A, t) \xrightarrow[A \gg 1]{} \frac{24\pi D}{5\gamma} A^{-2} h\left(\frac{A}{Dt}\right), \qquad [20]$$

where the scaling function $h(z)$ satisfies the conditions $h(z \ll 1) = 1$ and $h(z \gg 1) \simeq 0$. It is not difficult to verify that expression is the only scaling compatible with Eq. **2**. These two results are consistent with the fact that, for each sample, typically $A(t) \sim L^2(t)$ at late times in the scaling regime. Our scaling predictions are in agreement with our Monte Carlo simulations (Fig. 2). The power-law behavior of $\mathrm{Prob}(A, t)$ implies that the average area is not representative of the typical behavior of the epidemic area, which is actually dominated by fluctuations and rare events, with likelihood given by expression **20**.

Supercritical Regime. When $R_0 > 1$, it is convenient to rewrite Eq. **9** in terms of $W(x_m, t) = 1 - Q(x_m, t)$:

$$\frac{\partial}{\partial t} W = D \frac{\partial^2}{\partial x_m^2} W + \gamma(R_0 - 1) W - \gamma R_0 W^2 \qquad [21]$$

starting from the initial condition $W(x_m, 0) = 0$ for all $x_m > 0$ (Fig. 3). From Eq. **10**, $\langle L(t) \rangle = 2\pi \int_0^\infty W(x_m, t) dx_m$ is just the area under the curve $W(x_m, t)$ vs. x_m up to a factor 2π. As $t \to \infty$, the system approaches a stationary state for all $R_0 \geq 1$, which can be obtained by setting $\partial_t W = 0$ in Eq. **21**. For $R_0 > 1$, the stationary solution $W(x_m, \infty)$ approaches the constant $1 - 1/R_0$ exponentially fast as $x_m \to \infty$, namely $W(x_m, \infty) - 1 + R_0^{-1} \to \exp[-x_m/\xi]$, with a characteristic length scale $\xi = \sqrt{D/\gamma(R_0 - 1)}$. However, for finite but large t, $W(x_m, t)$ as a function of x_m has a two-step form: it first decreases from 1 to its asymptotic stationary value $1 - 1/R_0$ over the length scale ξ, and then decreases rather sharply from $1 - 1/R_0$ to 0. The frontier between the stationary asymptotic value $1 - 1/R_0$ (stable) and 0 (unstable) moves forward with time at constant velocity, thus

creating a traveling front at the right end, which separates the stationary value $1 - 1/R_0$ to the left of the front and 0 to the right. This front advances with a constant velocity v^* that can be estimated using the standard velocity selection principle (28–30). Near the front, where the nonlinear term is negligible, the equation admits a traveling front solution: $W(x_m, t) \sim \exp[-\lambda(x_m - vt)]$, with a one parameter family of possible velocities $v(\lambda) = D\lambda + \gamma(R_0 - 1)/\lambda$, parametrized by λ. This dispersion relation $v(\lambda)$ has a minimum at $\lambda = \lambda^* = \sqrt{\gamma(R_0 - 1)/D}$, where $v^* = v(\lambda^*) = 2\sqrt{D\gamma(R_0 - 1)}$. According to the standard velocity selection principle (28–30), for a sufficiently sharp initial condition, the system will choose this minimum velocity v^*. The width of the front remains $\sim\mathcal{O}(1)$ at large t. Thus, because of this sharpness of the front, to leading order for large t, one can approximate $W(x_m, t) \simeq (1 - 1/R_0)\Theta(v^*t - x_m)$ near the front. Hence, to leading order for large t, one gets $\langle x_m(t)\rangle \simeq (1 - 1/R_0)v^*t$ and $\langle x_m^2\rangle \simeq (1 - 1/R_0)(v^*t)^2$. The former gives, from Eq. **5**, the result announced in Eq. **3**. For the mean area in Eq. **7**, the term $\langle x_m^2\rangle \sim t^2$ for large t dominates over $\langle t_m\rangle \sim t$ (which can be neglected), and we get the result announced in Eq. **3**.

Conclusions

In this paper, we have developed a general procedure for assessing the time evolution of the convex hull associated with the outbreak of an epidemic. We find it extremely appealing that one can successfully use mathematical formulae (Cauchy) from 2D integral geometry to describe the spatial extent of an epidemic outbreak in relatively realistic situations. Admittedly, there are many assumptions in this epidemic model that are not quite realistic. For instance, we have ignored the fluctuations of the susceptible populations during the early stages of the epidemic: this hypothesis clearly breaks down at later times, when depletion effects begin to appear because of the epidemic invading a thermodynamical fraction of the total population. In addition, we have assumed that the susceptible individuals are homogeneously distributed in space, which is not the case in reality. Nonetheless, it must be noticed that, in practical applications, whenever strong heterogeneities appear, such as mountains, deserts, or oceans, one can split the analysis of the evolving phenomena by conveniently resorting to several distinct convex hulls—one for each separate region. For analogous reasons, the convex hull approach would not be suitable to characterize birth–death processes with long-range displacements, such as for instance branching Lévy flights.

The model discussed in this paper based on branching Brownian motion is amenable to exact results. More generally, realistic models could be taken into account by resorting to cumbersome Monte Carlo simulations. The approach proposed in this paper paves the way for assessing the spatial dynamics of the epidemic by more conveniently solving two coupled nonlinear equations under the assumption that the underlying process be rotationally invariant.

We conclude with an additional remark. In our computations of the mean perimeter and area, we have averaged over all realizations of the epidemics up to time t, including realizations that are already extinct at time t. It would also be interesting to consider averages only over the ensemble of epidemics that are still active at time t. In this case, we expect different scaling laws for the mean perimeter and the mean area of the convex hull. In particular, in the critical case, we believe that the behavior would be much closer to that of a regular Brownian motion.

ACKNOWLEDGMENTS. S.N.M. acknowledges support from Agence Nationale de la Recherche (ANR) Grant 2011-BS04-013-01 WALKMAT. S.N.M. and A.R. acknowledge support from the Indo-French Centre for the Promotion of Advanced Research under Project 4604-3.

1. Bailey NTJ (1975) *The Mathematical Theory of Infectious Diseases and Its Applications* (Griffin, London).
2. McKendrick AG (1925) Applications of mathematics to medical problems. *Proc Edinburgh Math Soc* 44(1):98–130.
3. Murray JD (1989) *Mathematical Biology* (Springer, Berlin).
4. Bartlett MS (1960) *Stochastic Population Models in Ecology and Epidemiology* (Wiley, New York).
5. Andersson H, Britton T (2000) *Stochastic Epidemic Models and their Statistical Analysis Lecture Notes in Statistics 151* (Springer, New York).
6. Antal T, Krapivsky PL (2012) Outbreak size distributions in epidemics with multiple stages. arXiv:1204.4214.
7. Anderson R, May R (1991) *Infectious Diseases: Dynamics and Control* (Oxford Univ Press, Oxford).
8. Antia R, Regoes RR, Koella JC, Bergstrom CT (2003) The role of evolution in the emergence of infectious diseases. *Nature* 426(6967):658–661.
9. Whittle P (1955) The outcome of a stochastic epidemic—a note on Bailey's paper. *Biometrika* 42(1/2):116–122.
10. Kendall DG (1956) Deterministic and stochastic epidemics in closed populations. *Proc 3rd Berkeley Symp Math Statist Prob* 4:149–165.
11. Bartlett MS (1956) *An Introduction to Stochastic Processes* (Cambridge Univ Press, Cambridge, United Kingdom).
12. Elliott P, Wakefield JC, Best NG, Briggs DJ (2000) *Spatial Epidemiology: Methods and Applications* (Oxford Univ Press, Oxford).
13. Radcliffe J (1976) The convergence of a position-dependent branching process used as an approximation to a model describing the spread of an epidemic. *J Appl Probab* 13(2):338–344.
14. Wang JS (1980) The convergence of a branching brownian motion used as a model describing the spread of an epidemic. *J Appl Probab* 17(2):301–312.
15. Riley S (2007) Large-scale spatial-transmission models of infectious disease. *Science* 316(5829):1298–1301.
16. Fraser C, et al. (2009) Pandemic potential of a strain of influenza A (H1N1): Early findings. *Science* 324(5934):1557–1561.
17. Colizza V, Barrat A, Barthélemy M, Vespignani A (2006) The role of the airline transportation network in the prediction and predictability of global epidemics. *Proc Natl Acad Sci USA* 103(7):2015–2020.
18. Brockmann D, Hufnagel L, Geisel T (2006) The scaling laws of human travel. *Nature* 439(7075):462–465.
19. Cowled B, Ward MP, Hamilton S, Garner G (2009) The equine influenza epidemic in Australia: Spatial and temporal descriptive analyses of a large propagating epidemic. *Prev Vet Med* 92(1–2):60–70.
20. Worton BJ (1995) A convex hull-based estimator of home-range size. *Biometrics* 51(4):1206–1215.
21. Giuggioli L, Abramson G, Kenkre VM, Parmenter RR, Yates TL (2006) Theory of home range estimation from displacement measurements of animal populations. *J Theor Biol* 240(1):126–135.
22. Randon-Furling J, Majumdar SN, Comtet A (2009) Convex hull of N planar Brownian motions: Exact results and an application to ecology. *Phys Rev Lett* 103(14):140602.
23. Majumdar SN, Comtet A, Randon-Furling J (2010) Random convex hulls and extreme value statistics. *J Stat Phys* 138(6):955–1009.
24. Cauchy A (1850) Mémoire sur la rectification des courbes et la quadrature des surfaces courbes. *Mém Acad Sci Paris* 22:3–15.
25. Santaló LA (1976) *Integral Geometry and Geometric Probability* (Addison–Wesley, Reading, MA).
26. Reymbaut A, Majumdar SN, Rosso A (2011) The convex hull for a random acceleration process in two dimensions. *J Phys A Math Theor* 44:415001.
27. Sawyer S, Fleischman J (1979) Maximum geographic range of a mutant allele considered as a subtype of a Brownian branching random field. *Proc Natl Acad Sci USA* 76(2):872–875.
28. van Saarloos W (2003) Front propagation into unstable states. *Phys Rep* 386(2–6):29–222.
29. Brunet E, Derrida B (2009) Statistics at the tip of a branching random walk and the delay of traveling waves. *Europhys Lett* 87:60010.
30. Majumdar SN, Krapivsky PL (2003) Extreme value statistics and traveling fronts: Various applications. *Physica A* 318(1–2):161–170.

Supporting Information

Dumonteil et al. 10.1073/pnas.1213237110

SI Text

1. Cauchy Formula. The problem of determining the perimeter and the area of the convex hull of any 2D stochastic process $[x(\tau), y(\tau)]$ with $0 \leq \tau \leq t$ can be mapped to the problem of computing the statistics of the maximum and the time of occurrence of the maximum of the 1D component process $x(\tau)$ (1, 2, 3). This goal is achieved by resorting to a formula by Cauchy, which applies to any closed convex curve C.

A sketch of the method is illustrated in Fig. S1. Choose the coordinates system such that the origin is inside the curve C, and take a given direction θ. For fixed θ, consider a stick perpendicular to this direction, and imagine bringing the stick from infinity; stop on first touching the curve C. At this point, the distance $M(\theta)$ of the stick from the origin is called the support function in the direction θ. Intuitively, the support function measures how close one can get to the curve C in the direction θ, coming from infinity. After the support function $M(\theta)$ is known, then Cauchy equations (4, 5) give the perimeter L and the area A enclosed by C, namely

$$L = \int_0^{2\pi} M(\theta) d\theta$$

and

$$A = \frac{1}{2} \int_0^{2\pi} \left[M^2(\theta) - \left(M'(\theta)\right)^2 \right] d\theta, \qquad \textbf{[S1]}$$

where $M'(\theta) = dM/d\theta$. For example, for a circle of radius $R = r$, $M(\theta) = r$, and one recovers the standard equations: $L = 2\pi r$ and $A = \pi r^2$. When C is the convex hull associated with the process at time t, we first need to compute its associated support function $M(\theta)$. A crucial point is to realize that actually $M(\theta) = \max_{0 \leq \tau \leq t}[x(\tau)\cos(\theta) + y(\tau)\sin(\theta)]$ (1, 2). Furthermore, if the process is rotationally invariant, any average is independent of the angle θ. Hence, for the average perimeter, we can simply set $\theta = 0$ and write $\langle L(t) \rangle = 2\pi \langle M(0) \rangle$, where brackets denote the ensemble average over realizations. Similarly, for the average area, $\langle A(t) \rangle = \pi[\langle M^2(0) \rangle - \langle M'(0)^2 \rangle]$. Clearly, $M(0) = \max_{0 \leq \tau \leq t}[x(\tau)]$ is then the maximum of the 1D component process $x(\tau)$ for $\tau \in [0, t]$. Assuming that $x(\tau)$ takes its maximum value $x(t_m)$ at time $\tau = t_m$ (Fig. 4), then, $M(0) = x(t_m) = x_m(t)$, and $M'(0) = y(t_m)$. [Actually, t_m implicitly depends on θ; hence, formally, $M'(\theta) = -x(t_m)\sin(\theta) + y(t_m)\cos(\theta) + \frac{dt_m}{d\theta}\frac{dz_\theta(t)}{dt}|_{t=t_m}$. Nonetheless, because $z_\theta(t)$ is maximum at $t = t_m$, by definition, $dz_\theta(t)/dt|_{t=t_m} = 0$.] Now, by taking the average over Cauchy formulas and using isotropy, we simply have Eqs. **5** and **6** from the text for the mean perimeter and the mean area of the convex hull C at time t. Note that this argument is very general and applicable to any rotationally invariant 2D stochastic process. Because the branching Brownian motion with death is rotationally invariant, we can use these formulae.

2. Numerical Methods. ***Numerical integration.*** Eqs. **9** and **14** in the text have been integrated numerically by finite differences in the following way. Time has been discretized by setting $t = ndt$, and space has been discretized by setting $x = idx$, where dt and dx are small constants. For the sake of simplicity, here, we consider the case $R_0 = 1$. We, thus, have

$$Q_{n+1}(i) = Q_n(i) + \gamma dt[1 - Q_n(i)]^2 + D\frac{dt}{(dx)^2}[Q_n(i+1) - 2Q_n(i) + Q_n(i-1)] \qquad \textbf{[S2]}$$

and

$$T_{n+1}(i) = T_n(i) + 2\gamma dt\ T_n(i)[Q_n(i) - 1] + D\frac{dt}{(dx)^2}[T_n(i+1) - 2T_n(i) + T_n(i-1)] + \frac{dt}{dx}[T_n(i) - T_n(i-1)]. \qquad \textbf{[S2]}$$

As for the initial conditions, $Q_0(0) = 0$, $Q_0(i > 0) = 1$, and $T_0(i) = 0\ \forall i$. The boundary conditions at the origin are $Q_n(0) = 0$ and $T_n(0) = 0$. To implement the boundary condition at infinity, we impose $Q_n(i_{\max}) = 1$ and $T_n(i_{\max}) = 0\ \forall n$, where the large value $i_{\max}$ is chosen so that $T_n(i_{\max}) - T_n(i_{\max} - 1) < 10^{-7}$. We have verified that numerical results do not change when passing to the tighter condition $T_n(i_{\max}) - T_n(i_{\max} - 1) < 10^{-9}$.

After $Q_n(i)$ and $T_n(i)$ are known, we use Eqs. **10** and **15** from the text to determine the average perimeter and area, respectively.

Monte Carlo simulations. The results of numerical integrations have been confirmed by running extensive Monte Carlo simulations. Branching Brownian motion with death has been simulated by discretizing time with a small dt: in each interval dt, with probability bdt, the walker branches and the current walker coordinates are copied to create a new initial point, which is then stored for being simulated in the next dt; with probability γdt, the walker dies and is removed, and with probability $1 - (b + \gamma)dt$, the walker diffuses: the x and y displacements are sampled from Gaussian densities of zero mean and SD $\sqrt{2Ddt}$, and the particle position is updated. The positions of all of the random walkers are recorded as a function of time, and the corresponding convex hull is then computed by resorting to the algorithm proposed in ref. 6.

Perimeter statistics. To complete the analysis of the convex hull statistics, in Figs. S2 and S3, we show the results for the perimeter.

3. Analysis of t_m. In the critical case $R_0 = 1$, the stationary joint probability density $P_\infty(x_m, t_m)$ satisfies (on setting $\partial P_t/\partial t = 0$ in Eq. **12** in the text)

$$\frac{\partial}{\partial t_m} P_\infty(x_m, t_m) = \left[D\frac{\partial^2}{\partial x_m^2} - \frac{2\gamma}{\left[1 + \sqrt{\frac{\gamma}{6D}} x_m\right]^2} \right] P_\infty(x_m, t_m). \qquad \textbf{[S4]}$$

For any $x_m > 0$, we have the condition $P_\infty(x_m, 0) = 0$. The boundary conditions for Eq. **S4** are $P_\infty(x_m \to \infty, t_m) = 0$ and $P_\infty(0, t_m) = q_\infty(0)\delta(t_m) = 2\sqrt{\gamma/(6D)}\delta(t_m)$. We first take the Laplace transform of Eq. **S4**, namely

$$\tilde{P}_\infty(x_m, s) = \int_0^\infty e^{-st_m} P_\infty(x_m, t_m) dt_m. \qquad \textbf{[S5]}$$

Hence, for all $x_m > 0$,

$$\frac{D}{s}\frac{\partial^2}{\partial x_m^2}\tilde{P}_\infty(x_m, s) = \left[1 + \frac{12}{\frac{s}{D}\left(\sqrt{\frac{6D}{\gamma}} + x_m\right)^2} \right] \tilde{P}_\infty(x_m, s), \qquad \textbf{[S6]}$$

where we have used the condition $P_\infty(x_m, 0) = 0$ for any $x_m > 0$. This second-order differential equation satisfies two boundary conditions: $\tilde{P}_\infty(\infty, s) = 0$ and $\tilde{P}_\infty(0, s) = 2\sqrt{\gamma/(6D)}$. The latter condition is obtained by Laplace transforming $P_\infty(0, t_m) = 2\sqrt{\gamma/(6D)}\delta(t_m)$. By setting

$$z = \left(\sqrt{\frac{6D}{\gamma}} + x_m\right)\sqrt{\frac{s}{D}}, \qquad \textbf{[S7]}$$

we rewrite the equation as

$$\frac{\partial^2}{\partial z^2}\tilde{P}_\infty - \tilde{P}_\infty - \frac{12}{z^2}\tilde{P}_\infty = 0. \qquad \textbf{[S8]}$$

On making the transformation $\tilde{P}_\infty(z) = \sqrt{z}F(z)$, the function $F(z)$ then satisfies the Bessel differential equation:

$$\frac{d^2}{dz^2}F(z) + \frac{1}{z}\frac{d}{dz}F(z) - \left[1 + \frac{49}{4z^2}\right]F(z) = 0. \qquad \textbf{[S9]}$$

The general solution of this differential equation can be expressed as a linear combination of two independent solutions: $F(z) = AI_{7/2}(z) + BK_{7/2}(z)$, where $I_\nu(z)$ and $K_\nu(z)$ are modified Bessel functions. Because $I_\nu(z) \sim e^z$ for large z, it is clear that, to satisfy the boundary condition $\tilde{P}_\infty(\infty, s) = 0$ [which means $F(z \to \infty) = 0$], we need to choose $A = 0$. Hence, we are left with $F(z) = BK_{7/2}(z)$, where the constant B is determined from the second boundary condition $\tilde{P}_\infty(0, s) = 2\sqrt{\gamma/(6D)}$. By reverting to the variable x_m, we finally get

$$\tilde{P}_\infty(x_m, s) = 2\sqrt{\frac{\gamma}{6D}}\sqrt{1 + \frac{\gamma}{6D}x_m}\,\frac{K_{7/2}\left[\left(\sqrt{\frac{6D}{\gamma}} + x_m\right)\sqrt{\frac{s}{D}}\right]}{K_{7/2}\left[\sqrt{\frac{6s}{\gamma}}\right]}. \qquad \textbf{[S10]}$$

Now, we are interested in determining the Laplace transform of the marginal density $\tilde{p}_\infty(s) = \int_0^\infty e^{-st_m} p_\infty(t_m)dt_m$, where $p_\infty(t_m) = \int_0^\infty P_\infty(x_m, t_m)dx_m$. Taking Laplace transform of this last relation with respect to t_m gives $\tilde{p}_\infty(s) = \int_0^\infty \tilde{P}_\infty(x_m, s)dx_m$. After we know $\tilde{p}_\infty(s)$, we can invert it to obtain $\mathrm{p}_\infty(t_m)$. Because we are interested only in the asymptotic tail of $\mathrm{p}_\infty(t_m)$, it suffices to investigate the small s behavior of $\tilde{p}_\infty(s)$. Integrating Eq. **S10** over x_m and taking the $s \to 0$ limit, we obtain, after some straightforward algebra,

$$\tilde{p}_\infty(s) = 1 + \frac{3}{5\gamma}s\,\ln(s) + \cdots. \qquad \textbf{[S11]}$$

We further note that

$$\int_0^\infty e^{-st_m} t_m^2 p_\infty(t_m)dt_m = \frac{d^2}{ds^2}\tilde{p}_\infty(s) \simeq \frac{3}{5\gamma s}, \qquad \textbf{[S12]}$$

which can then be inverted to give the following asymptotic behavior for large t_m:

$$p_\infty(t_m) \simeq \frac{3}{5\gamma t_m^2}. \qquad \textbf{[S13]}$$

Analogously as for $\langle x_m^2\rangle$, the moment $\langle t_m\rangle \to \infty$ because of the power-law tail $p_\infty(t_m) \propto t_m^{-2}$. Hence, we need to compute $\langle t_m\rangle$ for large but finite t: in this case, the time-dependent solution displays a scaling behavior:

$$p_t(t_m) \simeq p_\infty(t_m)g\left(\frac{t_m}{t}\right), \qquad \textbf{[S14]}$$

where the scaling function $g(z)$ satisfies the conditions $g(z \ll 1) \simeq 1$ and $g(z \gg 1) = 0$. Much like in expression **17** in the text for the marginal density $q_t(x_m)$, we have a power-law tail of $p_t(t_m)$ for large t_m that has a cutoff at a scale $t_m^* \sim t$, and $g(z)$ is the cutoff function. As in the case of x_m, we do not need the precise form of $g(z)$ to compute the leading term of the first moment $\langle t_m\rangle = \int_0^\infty p_t(t_m)t_m dt_m$ for large t. Cutting off the integral at $t_m^* = c_1 t$ [where c_1 depends on the precise form of $g(z)$] and performing the integration gives

$$\langle t_m\rangle \simeq \int_0^t t_m p_\infty(t_m)dt_m \simeq \frac{3}{5\gamma}\,\ln t, \qquad \textbf{[S15]}$$

which is precisely the result announced in expression **19** in the text.

1. Randon-Furling J, Majumdar SN, Comtet A (2009) Convex hull of N planar Brownian motions: Exact results and an application to ecology. *Phys Rev Lett* 103(14): 140602.
2. Majumdar SN, Comtet A, Randon-Furling J (2010) Random convex hulls and extreme value statistics. *J Stat Phys* 138(6):955–1009.
3. Cauchy A (1850) Mémoire sur la rectification des courbes et la quadrature des surfaces courbes. *Mém Acad Sci Paris* 22:3–15.
4. Santaló LA (1976) *Integral Geometry and Geometric Probability* (Addison–Wesley, Reading, MA).
5. Reymbaut A, Majumdar SN, Rosso A (2011) The convex hull for a random acceleration process in two dimensions. *J Phys A Math Theor* 44:415001.
6. Gehrman DC (2005) Module: Finding the convex hull of a set of 2D points. *Python Cookbook*, eds Martelli A, Ravenscroft A, Ascher D (O'Reilly, Paris).

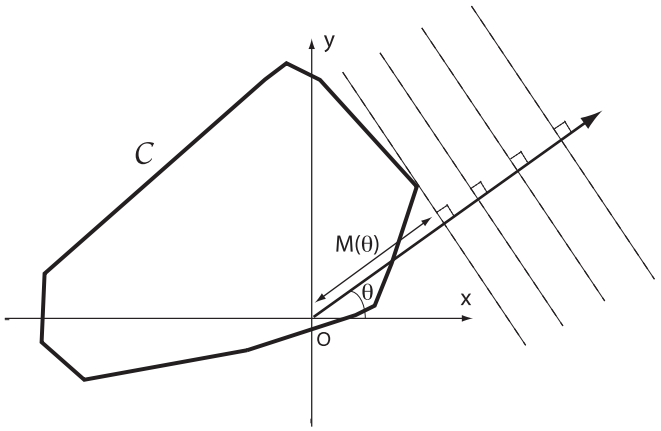

Fig. S1. Cauchy construction of the 2D convex hull, with support function $M(\theta)$ representing the distance along the direction θ.

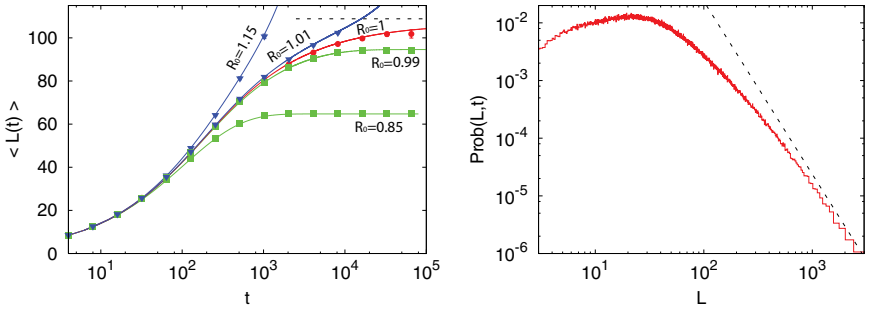

Fig. S2. (*Left*) The average perimeter $\langle L(t)\rangle$ of the convex hull as a function of the observation time. For the parameter values, we have chosen $D = 1/2$ and $b = R_0\gamma = 0.01$. We considered five different values of R_0. We have obtained these results by two different methods. (*i*) One method is by the numerical integration of Eq. **S9** and using Eq. **10** in the text (with the choices $dt = 0.003125$ and $dx = 0.1768$). These results are displayed as solid lines. (*ii*) Another method is by Monte Carlo simulations of the 2D branching Brownian motion with death with the same parameters and the choice of the Monte Carlo time step $dt = 0.25$ with the results averaged over 10^5 samples. Monte Carlo simulations are displayed as symbols. The dashed lines represent the asymptotic limits as given in Eq. **1** in the text for the critical case $R_0 = 1$. (*Right*) Distribution of the perimeter of the convex hull for the critical case $R_0 = 1$, with $\gamma = 0.01$ and $D = 1/2$, as obtained by Monte Carlo simulations with time step $dt = 1$ and $t = 4 \times 10^5$. The number of realizations is 2×10^6. The dashed line in *Right* corresponds to the power-law L^{-3} (up to an arbitrary prefactor).

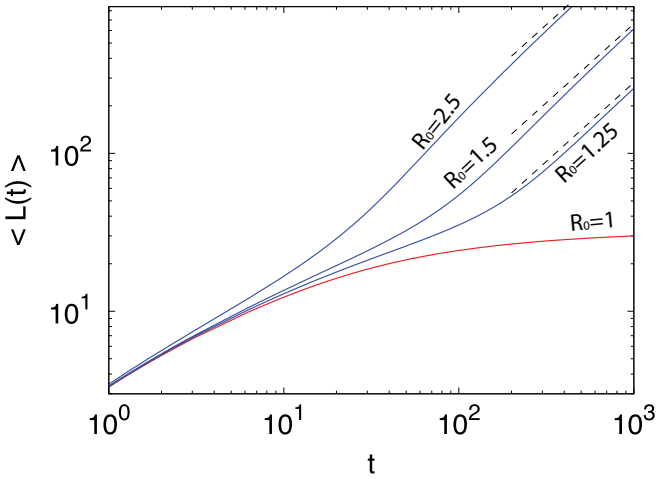

Fig. S3. The time behavior of the average perimeter in the supercritical regime for different values of $R_0 > 1$. Dashed lines represent the asymptotic scaling as in Eq. **3** in the text. The red curve corresponds to the critical regime.